ISSN 1392–1320 MATERIALS SCIENCE (MEDŽIAGOTYRA). Vol. 21, No. 2. 2015

Investigation of the Crystal Structure, Dielectric, Electrical and Microstructural Properties of Cobalt-containing Calcium Orthophosphates

Omer KAYGILI [1] *, Sergey V. DOROZHKIN [2], Serhat KESER [3], Fahrettin YAKUPHANOGLU [1]

[1] *Department of Physics, Faculty of Science, Firat University, Elazig 23119, Turkey*
[2] *Kudrinskaja Square 1-155, Moscow 123242, Russia*
[3] *Department of Chemistry, Faculty of Science, Firat University, Elazig 23119, Turkey*

crossref http://dx.doi.org/10.5755/j01.mm.21.2.6251

Received 20 January 2014; accepted 17 April 2014

Pure hydroxyapatite and cobalt-containing calcium orthophosphate ceramics were synthesized by the sol-gel method and their properties were analyzed by Fourier transform infrared spectroscopy, X-ray diffraction, dielectric impedance spectroscopy and scanning electron microscopy techniques. The average crystallite size of the samples was found to be 30 nm – 56 nm. The crystallinity decreased gradually with the addition of Co. The resistance values were found to be ~10^{12} Ω. Dielectric permittivity and alternating current conductivity of all the samples showed substantial changes in the presence of cobalt. The morphology and particle size distribution of all the samples were changed with increasing amount of Co. In addition, the high content of Co ions was found to both destroy the apatitic structure of the hydroxyapatite and cause the calcium deficiency. The results indicated that, in presence of high amounts of Co, $Ca_{9.5}Co(PO_4)_7$ ceramics could be prepared.
Keywords: ceramics, sol-gel method, X-ray diffraction (XRD), crystal structure, dielectric properties.

1. INTRODUCTION

Ceramics have been widely used in medicine for many years, due to highly desirable characteristics, such as biocompatibility, non-toxicity and chemical stability [1 – 3]. Among the available ceramic materials, hydroxyapatite (HAP, $Ca_{10}(PO_4)_6(OH)_2$) and other calcium orthophosphates have a special importance for medicine due to their chemical and structural similarities with the inorganic part of bones and teeth of mammals [4, 5]. Therefore, a number of techniques, such as sol-gel method [6], solid-state reaction [7], hydrothermal synthesis [8] and chemical co-precipitation [9] have been used for the synthesis of HAP. Among these techniques, sol-gel method is extremely preferred because of its advantages (e. g., inexpensive precursors, high product purity and low synthesis temperature) [10, 11].

Cobalt (Co) and its alloys have been extremely used in biotechnology due to the useful mechanical properties [12, 13]. So far, only a few studies have been reported on using of Co as a dopant in HAP structure [14 – 20]. The authors of those studies used small amounts of Co and preserved the HAP structure. In the present study, we decided to increase the amount of Co and prepared cobalt–containing calcium orthophosphates with various atomic percentages of Co (10, 20, 25, 30 and 40 at.%) and investigated their chemical, electrical, dielectric and microstructural properties.

* Corresponding author. Tel. :+90-424-2370000 / 3623; fax.: +90-424-2330062. E-mail address: okaygili@firat.edu.tr (O. Kaygili)

2. EXPERIMENTAL DETAILS

2.1. Sol-gel synthesis

Both Co-containing calcium orthophosphates and HAP were synthesized by the sol-gel method. The preparation procedure is described in the flowchart (Fig. 1).

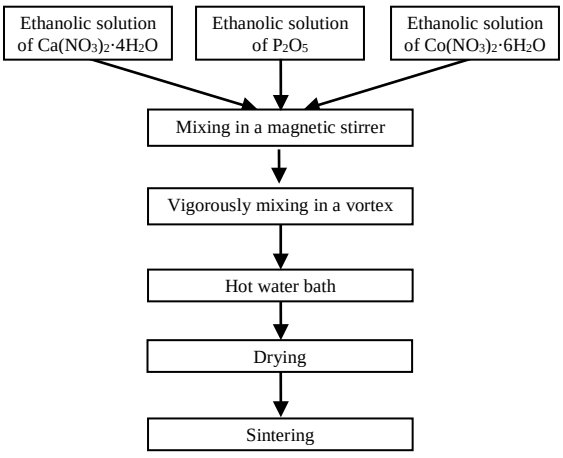

Fig. 1. Flowchart of the cobalt-containing calcium orthophosphate ceramics by sol-gel method

The used precursors were the calcium nitrate tetrahydrate ($Ca(NO_3)_2.4H_2O$, Merck), phosphorus pentoxide (P_2O_5, Merck) and cobalt (II) nitrate hexahydrate ($Co(NO_3)_2.6H_2O$, Merck). The Co-content of the samples was chosen as 0, 10, 20, 25, 30 and 40 at.%, and these samples were named as HAP, 10 % Co, 20 % Co, 25 %

Co, 30 % Co and 40 % Co, respectively. Both Ca/P and (Ca + Co)/P molar ratios were adjusted to 1.67 for preparation of HAP and Co-containing calcium orthophosphate samples, respectively. The nominal quantities of the precursors were dissolved in anhydrous ethanol (C_2H_5OH, Sigma-Aldrich) and the solutions were stirred using a magnetic stirrer at room temperature for 30 min. Then, the solutions were mixed under vigorous stirring using a vortex mixer and the prepared mixtures kept stirring for 10 min. Afterwards, the mixtures were heated in a hot-water bath at 60 °C for 2 h. The obtained gels were dried in an oven at 120 °C during 15 h and the dry powders were calcined in a furnace at 900 °C for 1 h.

2.2. Characterization methods

FTIR spectra of the samples were performed on a Perkin Elmer spectrophotometer in the frequency interval of 400 cm^{-1} – 4000 cm^{-1} using the KBr pellet. X-ray diffractometer (XRD, Bruker D8 Advance, CuKα) was used for phase identification and to analyze the crystal structures of the samples. The measurements were performed in the range of 15° – 70° with a step of 0.02° s^{-1}. The average crystallite size (D) for the ceramic samples was determined by the following Debye-Scherrer equation [21]

$$D = \frac{0.9\lambda}{\beta \cos\theta}\ , \qquad (1)$$

where λ is the wavelength for CuKα radiation) of the X-ray, β is the full width at half maximum (FWHM) of X-ray reflection in radian, θ is the Bragg's diffraction angle in degree. The dielectric measurements of the samples were obtained by a Hioki 3532-50 LCR HiTESTER at frequencies between 50 Hz and 5 MHz at room temperature by placing the pellet samples between two parallel plate electrodes. The morphology of the as-synthesized samples was investigated using a scanning electron microscope (SEM, ZEISS EVO 50) operated at an accelerating voltage of 15 kV, coupled with EDX (OXFORD Inca Energy 350).

3. RESULTS AND DISCUSSION

3.1. Fourier transform infrared (FTIR) spectroscopy

The FTIR spectra of the ceramic samples show the characteristic bands of hydroxyl and phosphate groups (Fig. 2). The observed bands at about 555 – 602, 960, 1047 and 1100 cm^{-1} are related to the phosphate group [22]. The libration band at 631 cm^{-1} for HAP and at 635 cm^{-1} for 40 %Co and the characteristic stretching band at 3641 cm^{-1} for all the samples were observed from FTIR spectra. For only HAP, another band belonging to the stretching mode of the hydroxyl group was also detected at 3571 cm^{-1}. The broad band at 3300 cm^{-1} – 3600 cm^{-1}, as well as the narrow band at 1635 cm^{-1}, corresponds to the adsorbed water [23]. Three weak bands belonging to the carbonate group were observed only for the Co-free sample. First band at 872 cm^{-1} corresponds to bending mode of the carbonate group. The other two bands at 1421 cm^{-1} and 1467 cm^{-1} are ascribed to stretching modes of the carbonate group in B– and A–type, respectively [24].

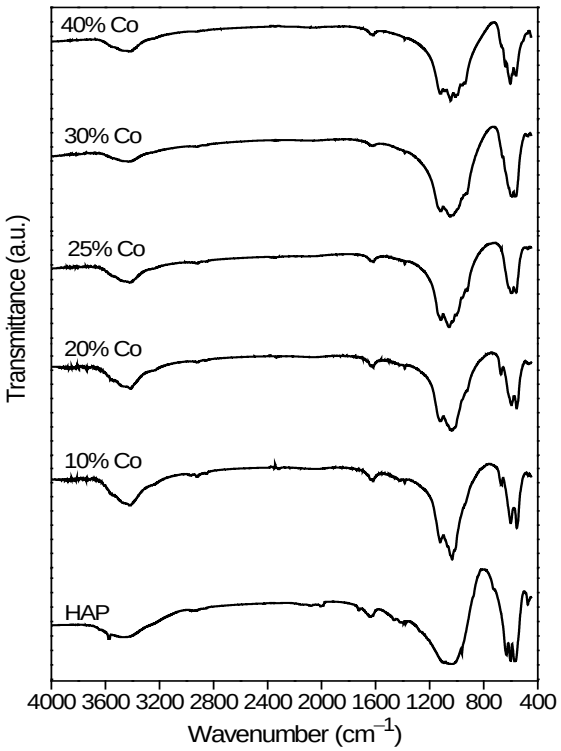

Fig. 2. FTIR spectra of the as-synthesized ceramic samples

3.2. Detailed crystal structure analysis

XRD patterns of the samples synthesized with various contents of Co are shown in Fig. 3. The obtained experimental patterns were analyzed and compared to the Joint Committee on Powder Diffraction and Standards (JCPDS) cards.

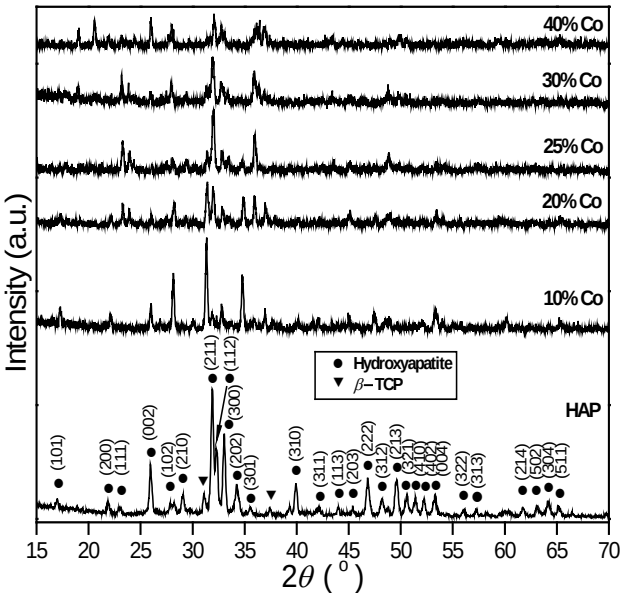

Fig. 3. XRD patterns of the as-synthesized ceramic samples (the unmarked peaks belong to $Ca_{9.5}Co(PO_4)_7$ phase)

As seen in Fig. 3, the ceramics are the polycrystalline materials. The calculated values of D and crystallinity (X_C) for all the samples are given in Table 1. For HAP sample, these values are in quite good agreement with the values obtained by Fathi et al. [24]. All the samples are formed from nanoparticles ranging from 30 nm to 56 nm.

Table 1. Calculated values of the crystallite size (D) and crystallinity degree (X_C)

Sample	D, nm	X_C
HAP	31.37	0.84
10 % Co	48.85	0.56
20 % Co	34.17	0.48
25 % Co	42.71	0.42
30 % Co	30.69	0.36
40 % Co	55.62	0.29

The crystallinity degree (X_C) of the ceramics was calculated from the ratio of the area under crystalline peaks to the total area under crystalline and amorphous peaks. As seen in Fig. 4 and Table 1, the presence of Co^{2+} ion, ranging from 10 at.% to 40 at.%, in HAP structure induces a significant decrease in the crystallinity from 0.56 to 0.29, which is in good agreement with Ignjatović et al. [19]. The crystallinity of the Co-containing samples is much lower than that of HAP (0.84). This indicates that the structure of the HAP was transformed to a new structure with high cobalt contents.

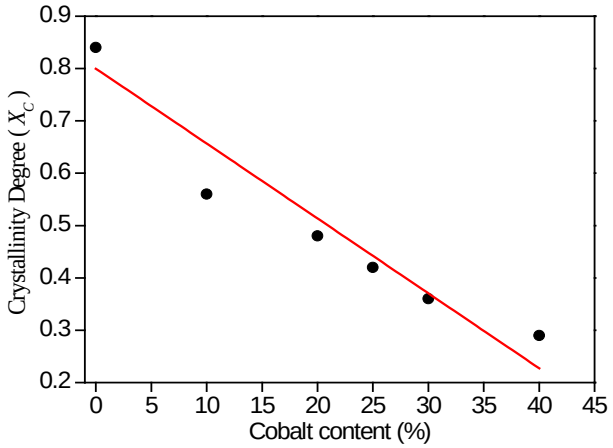

Fig. 4. Plot of crystallinity degree vs. Co content for the as-synthesized ceramics

The lattice parameters of the ceramic samples were calculated using the following equations (2) and (3), belonging to hexagonal and rhombohedral crystal systems respectively [25]

$$\frac{1}{d^2} = \frac{4}{3}\left(\frac{h^2+hk+k^2}{a^2}\right) + \frac{l^2}{c^2}, \quad (2)$$

$$\frac{1}{d^2} = \frac{\left(h^2+k^2+l^2\right)\sin^2\alpha + 2(hk+kl+hl)(\cos^2\alpha-\cos\alpha)}{a^2(1-3\cos^2\alpha+2\cos^3\alpha)}, \quad (3)$$

where d is the distance for two adjacent plane, a and c are the lattice parameters, h, k and l are the Miller indices, and α is the lattice angle for rhombohedral structure.

The calculated values of the lattice parameters for all the samples are given in Table 2. The lattice parameters of Co including samples show a tremendous increase with respect to the HAP. This confirms that the HAP structure was destroyed in all over of the studied composition area (10 % – 40 % Co). The formation of a new calcium cobalt phosphate phase identified as $Ca_{9.5}Co(PO_4)_7$ (JCPDS, Pdf Number: 89-5586) is observed. The addition of Co in high rates causes to crystal structure transformation from hexagonal to rhombohedral.

Table 2. Lattice parameters of the as-synthesized ceramic samples

Sample	a, nm	c, nm
HAP (JCPDS 09-432)	0.942	0.688
HAP	0.938	0.686
10 % Co	1.031	3.675
20 % Co	1.027	3.667
25 % Co	1.031	3.667
30% Co	1.033	3.884
40 % Co	1.043	3.635

3.3. Electrical and dielectric properties

Figs. 5, 6, 7 and 8 show the impedance (Z), alternating current conductivity (σ_{ac}), $\log\sigma_{ac}$ vs. $\log\omega$ curve and dielectric permittivity (ε') values of all the samples as a function of frequency. As can be seen in Fig. 5, with increasing the frequency, impedance values of the samples dramatically decreased from ~70 MΩ to ~2 kΩ. Moreover, the impedance values of the Co-doped samples are higher than that of HAP.

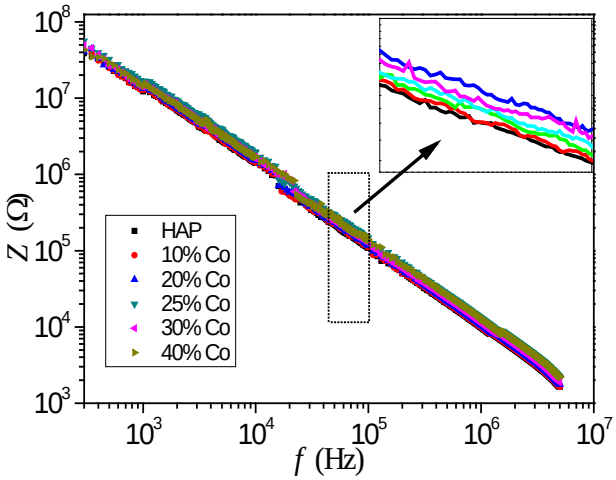

Fig. 5. Plots of impedance vs. frequency of the as-synthesized ceramic samples

From Fig. 6, the alternating current conductivity (σ_{ac}) values of the samples rise with the frequency increasing. The ac conductivity (σ_{ac}) mechanism of all samples was analyzed by the following equation known as the ac universality law [26]

$$\sigma_{ac} = \sigma_{dc} + B\omega^s, \quad (4)$$

where σ_{dc} is the direct current conductivity, B is a constant, ω is the angular frequency and s is an exponent. The s values were calculated from the slope of $\log\sigma$ vs. $\log\omega$ graph (Fig. 7). These values are about equal to 1 for all samples. This can be explained as follows: the resistance values of all samples are about 10^{12} Ω, and they exhibit the insulator behavior. Since there is no measurable direct current conductivity (σ_{dc}) of all ceramic samples, the s value is close to 1 [27]. This result indicates that the hopping motion involves a translational motion with a sudden hopping [28].

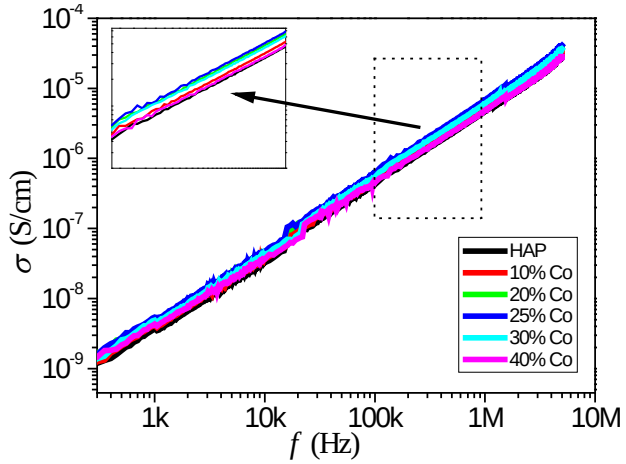

Fig. 6. Plots of alternating current conductivity as a function of frequency for the as-synthesized ceramic samples

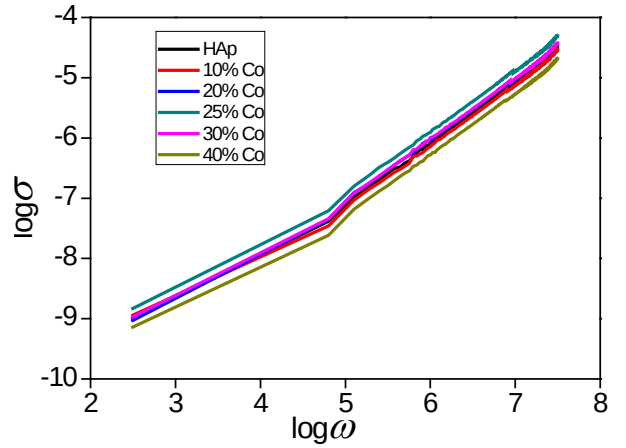

Fig. 7. Plots of logσ vs. logω for all the as-synthesized ceramic samples

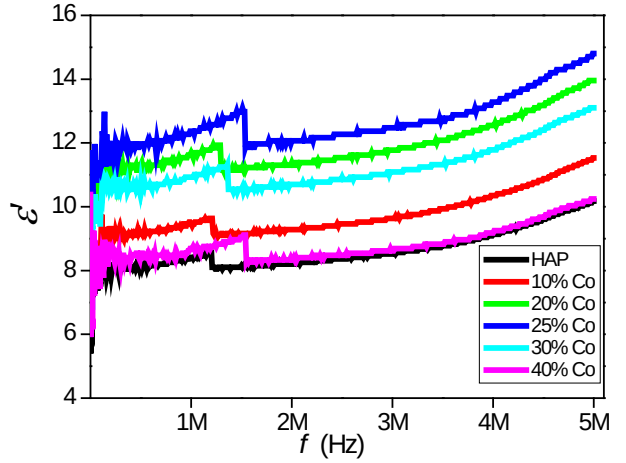

Fig. 8. Plots of dielectric permittivity vs. frequency of the as-synthesized ceramic samples

The values of dielectric permittivity (ε') were evaluated from

$$\varepsilon' = \frac{Ct}{\varepsilon_0 A}, \quad (5)$$

where C and t are the capacitance and thickness of the sample, ε_0 is the permittivity of the vacuum and A is the area of cross-section of the sample [29]. Although the values of dielectric permittivity (ε') for all the samples are almost constant until 10 kHz, ε' shows an increase at the higher frequencies than this value (Fig. 8 and Table 3).

Table 3. The dielectric permittivity values of the ceramic samples for different frequencies

Sample	$\varepsilon'_{1\ kHz}$	$\varepsilon'_{100\ kHz}$	$\varepsilon'_{1\ MHz}$	$\varepsilon'_{5\ MHz}$
HAP	6.75	7.58	8.41	10.18
10 % Co	7.39	8.51	9.46	11.53
20 % Co	9.28	10.60	11.69	13.96
25 % Co	9.77	10.95	12.37	14.81
30 % Co	8.84	9.77	10.93	13.10
40 % Co	7.77	8.12	8.69	10.24

For 1 kHz frequency, the dielectric permittivity of HAP was found to be 6.75 and this value is in agreement with the reported dielectric permittivity values in the literature [18, 30 – 32]. The ε' values of all samples at 1 kHz frequency were found to be 7.39, 9.28, 9.77, 8.84 and 7.77 for 10 % Co, 20 % Co, 25 % Co, 30 % Co and 40 % Co, respectively. While the ε' values are decreased significantly with the increase of the frequency for Zn doped HAP based ceramics [29], the fluctuations are seen with the increasing frequency for Mg doped HAP based ceramics [33], whereas in this study, the dielectric permittivity values of Co-doped HAP based calcium orthophosphates increases with the increasing frequency. Our results show that the dielectric properties of the cobalt-containing calcium orthophosphate ceramics may be controlled by Co content. The ε' values of the Co including ceramic samples are higher than the HAP sample. This behavior may be resulted from the presence of the rhombohedral phase in ceramics.

3.4. Scanning electron microscope observations of microstructures

Fig. 9 shows the morphologies of the as-prepared samples at the magnification of 5000×. With the addition of Co, the microstructure and particle size distribution are changed. The morphology and crystal structure are affected by the increasing amount of Co, which are in good agreement with Ignjatović et al. [24]. Without any impurity, Ca, Co, O and P are detected from the energy dispersive X-ray (EDX) analysis and these results are given in Table 4.

Table 4. The energy dispersive X-ray (EDX) analysis reports of all the samples

Sample	Ca, at.%	Co, at.%	O, at.%	P, at.%
HAP	23.60	–	62.07	14.33
10 % Co	19.39	4.19	64.72	11.69
20 % Co	15.81	9.95	58.26	15.98
25 % Co	10.45	14.28	60.17	15.10
30 % Co	8.80	15.75	59.10	16.35
40 % Co	4.16	22.19	60.35	13.31

The Ca/P molar ratio of the HAP is found to be 1.65, and this ratio is so close to that of the 1.67 value belonging to the stoichiometric hydroxyapatite [4, 5]. The (Ca + Co)/P molar values are also found to be 2.02, 1.61, 1.64, 1.50 and

1.98 for 10 % Co, 20 % Co, 25 % Co, 30 % Co and 40 % Co, respectively. The (Ca + Co)/P ratio is changed with the addition of Co, and except for 20 % Co and 25 % Co, this ratio is different than the expected value for all the Co-containing samples. Co substitution and Ca-deficiency are gradually increased with the amount of Co. Additionally, the Co/(Ca + Co) molar values are also found to be 0.18, 0.39, 0.58, 0.64 and 0.84 for 10 % Co, 20 % Co, 25 % Co, 30 % Co and 40 % Co, respectively. This is an expected result and supports that Co incorporation in the apatitic structure increases with the addition of Co. Since Co^{2+} ions have a smaller ionic radius (0.074 nm) than those of Ca^{2+} ions (0.099 nm), Co^{2+} ions can be substituted with Ca^{2+} ions [34].

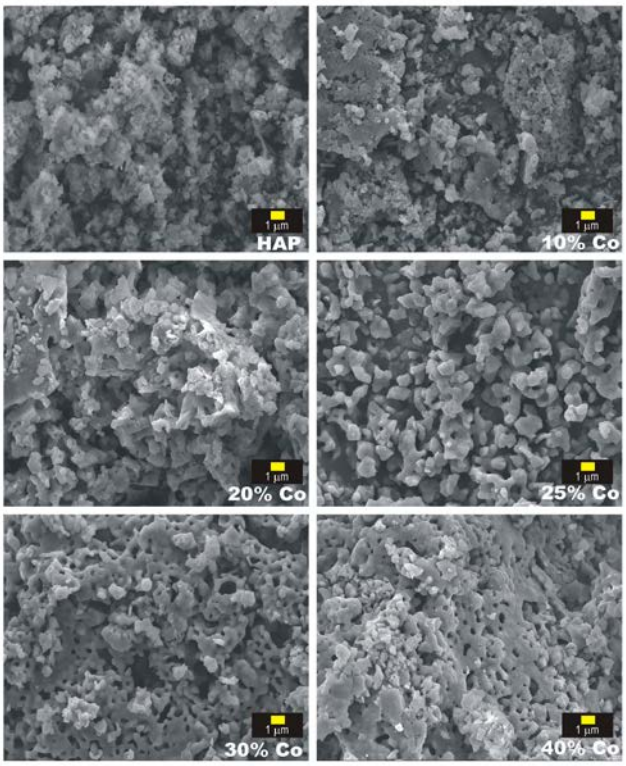

Fig. 9. SEM images of the as-synthesized ceramic samples at 5000× magnification

4. CONCLUSIONS

The cobalt-containing calcium orthophosphate ceramics with various atomic percentages of Co (10, 20, 25, 30 and 40 at.%) were prepared. The crystallinity degree of Co-containing ceramics was found to decrease with increasing molar ratio of Co. Since the resistance values of all samples were about 10^{12} Ω, they exhibited the insulator behavior. With the increasing frequency, while the impedance values were decreased, the alternating current conductivities were increased. In comparison to HAP, the addition of Co at the high molar ratios affected the dielectric properties of the ceramic samples, and these properties could be controlled by Co content. The microstructure and particle size distribution were changed with the addition of Co. The high content of Co ions destroyed the apatitic structure of the HAP and caused the calcium deficiency. The obtained results indicated that in presence of high amounts of Co, $Ca_{9.5}Co(PO_4)_7$ ceramics might be prepared.

REFERENCES

1. **Kokubo, T.** Bioceramics and Their Clinical Applications. CRC Press, Boca Raton, 2008.
2. **Park, J.** Bioceramics: Properties, Characterizations, and Applications. Springer, New York, 2008.
3. **Hench, L. L.** An Introduction to Bioceramics. Imperial College Press, London, 2013. http://dx.doi.org/10.1142/p884
4. **LeGeros, R. Z.** Calcium Phosphates in Oral Biology and Medicine. Karger, Basel, 1991. http://dx.doi.org/10.1159/issn.0077-0892
5. **Dorozhkin, S. V.** Calcium Orthophosphates: Applications in Nature, Biology, and Medicine. Pan Stanford, 2012. http://dx.doi.org/10.1201/b12312
6. **Padmanabhan, S. K., Balakrishnan, A., Chu, M. C., Lee, Y. J., Kim, T. N., Cho, S. J.** Sol-gel Synthesis and Characterization of Hydroxyapatite Nanorods *Particuology* 7 2009: pp. 466 – 470.
7. **Farzadi, A., Solati-Hashjin, M., Bakhshi, F., Aminian, A.** Synthesis and Characterization of Hydroxyapatite/ β-tricalcium Phosphate Nanocomposites Using Microwave Irradiation *Ceramics International* 37 2011: pp. 65 – 71. http://dx.doi.org/10.1016/j.ceramint.2010.08.021
8. **Liu, F., Wang, F., Shimizu, T., Igarashi, K., Zhao, L.** Hydroxyapatite Formation on Oxide Films Containing Ca and P by Hydrothermal Treatment *Ceramics International* 32 2006: pp. 527 – 531.
9. **Kumar, R., Prakash, K. H., Cheang, P., Khor, K. A.** Temperature Driven Morphological Changes of Chemically Precipitated Hydroxyapatite Nanoparticles *Langmuir* 20 2004: pp. 5196 – 5200.
10. **Franco, P. Q., João, C. F. C., Silva, J. C., Borges, J. P.** Electrospun Hydroxyapatite Fibers from a Simple Sol-gel System *Materials Letters* 67 2012: pp. 233 – 236.
11. **Feng, W., Mu-sen, L., Yu-peng, L., Yong-xin, Q.** A Simple Sol-gel Technique for Preparing Hydroxyapatite Nanopowders *Materials Letters* 59 2005: pp. 916 – 919.
12. **Escobedo, J. C., Ortiz, J. C., Almanza, J. M., Cortés, D. A.** Hydroxyapatite Coating on a Cobalt Base Alloy by Investment Casting *Scripta Materialia* 54 2006: pp. 1611 – 1615.
13. **Müller, R., Abke, J., Schnell, E., Scharnweber, D., Kujat, R., Englert, C., Taheri, D., Nerlich, M., Angele, P.** Influence of Surface Pretreatment of Titanium- and Cobalt-based Biomaterials on Covalent Immobilization of Fibrillar Collagen *Biomaterials* 27 2006: pp. 4059 – 4068.
14. **Mabilleau, G., Filmon, R., Petrov, P. K., Baslé, M. F., Sabokbar, A., Chappard, D.** Cobalt, Chromium and Nickel Affect Hydroxyapatite Crystal Growth in vitro *Acta Biomaterialia* 6 2010: pp. 1555 – 1560. http://dx.doi.org/10.1016/j.actbio.2009.10.035
15. **Petchsang, N., Pon-On, W., Hodak, J. H., Tang, I. M.** Magnetic Properties of Co-ferrite-doped Hydroxyapatite Nanoparticles having a Core/shell Structure *Journal of Magnestism and Magnetic Materials* 321 2009: pp. 1990 – 1995.
16. **Stojanović, Z., Veselinović, L., Marković, S., Ignjatović, N., Uskoković, D.** Hydrothermal Synthesis of Nanosized Pure and Cobalt-exchanged Hydroxyapatite *Materials and Manufacturing Processes* 24 2009: pp. 1096 – 1103.

17. **Veselinović, L., Karanović, L., Stojanović, Z., Bracko, I., Marković, S., Ignjatović, N., Uskoković, D.** Crystal Structure of Cobalt-substituted Calcium Hydroxyapatite Nanopowders Prepared by Hydrothermal Processing *Journal of Applied Crystallography* 43 2010: pp. 320 – 327.
18. **Hontsu, S., Matsumoto, T., Ishii, J., Nakamori, M., Tabata, H., Kawai, T.** Electrical Properties of Hydroxyapatite Thin Films Grown by Pulsed Laser Deposition *Thin Solid Films* 295 1997: pp. 214 – 217.
19. **Ignjatović, N., Ajduković, Z., Savić, V., Najman, S., Mihailović, D., Vasiljević, P., Stojanović, Z., Uskoković, V., Uskoković, D.** Nanoparticles of Cobalt-substituted Hydroxyapatite in Regeneration of Mandibular Osteoporotic Bones *Journal of Materials Science: Materials in Medicine* 24 2013: pp. 343 – 354. http://dx.doi.org/10.1007/s10856-012-4793-1
20. **Tank, K. P., Chudasama, K. S., Thaker, V. S., Joshi, M. J.** Cobalt-doped Nanohydroxyapatite: Synthesis, Characterization, Antimicrobial and Hemolytic Studies *Journal of Nanoparticle Research* 15 2013: p. 1644. http://dx.doi.org/10.1007/s11051-013-1644-z
21. **Figueiredo, M., Fernando, A., Martins, G., Freitas, J., Judas, F., Figueiredo, H.** Effect of the Calcination Temperature on the Composition and Microstructure of Hydroxyapatite Derived from Human and Animal Bone *Ceramics International* 36 2010: pp. 2383 – 2393.
22. **Koutsopoulos, S.** Synthesis and Characterization of Hydroxyapatite Crystals: A Review Study on the Analytical Methods *Journal of Biomedical Materials Research* 62 2002: pp. 600 – 612.
23. **Rodrigues, C. V. M., Serricella, P., Linhares, A. B. R., Guerdes, R. M., Borojevic, R., Rossi, M. A., Duarte, M. E. L., Farina, M.** Characterization of a Bovine Collagen-hydroxyapatite Composite Scaffold for Bone Tissue Engineering *Biomaterials* 24 2003: pp. 4987 – 4997.
24. **Fathi, M. H., Hanifi, A., Mortazavi, V.** Preparation and Bioactivity Evaluation of Bone-like Hyroxyapatite Nanopowder *Journal of Materials Processing Technology* 202 2008: pp. 536 – 542.
25. **Cullity, B. D.** Elements of X-ray Diffraction. Addison-Wesley Publishing Company, Massachussets, 1978.
26. **Pollak, M., Geballe, T. H.** Low-frequency Conductivity due to Hopping Processes in Silicon *Physical Review* 122 1961: pp. 1742 – 1753.
27. **Dyre, J. C., Schrøder, T. B.** Universality of ac Conduction in Disordered Solids *Reviews of Modern Physics* 72 2000: pp. 873 – 892.
28. **Funke, K.** Jump Relaxation in Solid Electrolytes *Progress in Solid State Chemistry* 22 1993: pp. 111 – 195. http://dx.doi.org/10.1016/0079-6786(93)90002-9
29. **Kaygili, O., Tatar, C.** The Investigation of Some Physical Properties and Microstructure of Zn-doped Hydroxyapatite Bioceramics Prepared by Sol-gel Method *Journal of Sol-Gel Science and Technology* 61 2012: pp. 296 – 309.
30. **Silva, C. C., Rocha, H. H. B., Freire, F. N. A., Santos, M. R. P., Saboia, K. D. A., Góes, J. C., Sombra, A. S. B.** Hydroxyapatite Screen-printed Thick Films: Optical and Electrical Properties *Materials Chemistry and Physics* 92 2005: pp. 260 – 268. http://dx.doi.org/10.1016/j.matchemphys.2005.01.028
31. **Silva, C. C., Valente, M. A., Graça, M. P. F., Sombra, A. S. B.** The Modulus Formalism Used in the Dielectric Analysis of Hydroxyapatite and Calcium Phosphate with Titanium Formed by Dry Ball Milling *Journal of Non-Crystalline Solids* 351 2005: pp. 2945 – 2950.
32. **Hoepfner, T. P., Case, E. D.** The Porosity Dependence of the Dielectric Constant for Sintered Hydroxyapatite *Journal of Biomedical Materials Research* 60 2002: pp. 643 – 650.
33. **Kaygili, O., Tatar, C., Yakuphanoglu, F.** Structural and Dielectrical Properties of Mg_3–$Ca_3(PO_4)_2$ Bioceramics Obtained from Hydroxyapatite by Sol-gel Method *Ceramics International* 38 2012: pp. 5713 – 5722.
34. **Zhang, M., Wu, C., Li, H., Yuen, J., Chang, J., Xiao, Y.** Preparation, Characterization and in vitro Angiogenic Capacity of Cobalt Substituted β-tricalcium Phosphate Ceramics *Journal of Materials Chemistry* 22 2012: pp. 21686 – 21694. http://dx.doi.org/10.1039/c2jm34395a